LA-UR-20-23734
Approved for public release; distribution is unlimited.

Title: Advanced Analysis of Plutonium: Pre- and Post-Detonation Scenarios

Author(s): Bishop, Jessica Lyn

Intended for: Report

Issued: 2020-05-19

Advanced Analysis of Plutonium: Pre- and Post-Detonation Scenarios

A Dissertation Presented for the Doctor of Philosophy
Degree in Nuclear Engineering
LA-UR-pending

Jessica L. Bishop

April 2020
Department of Nuclear Engineering | Tickle College of Engineering
University of Tennessee, Knoxville

Committee Members:

Dr. Maik K. Lang (committee chair)	*Associate Professor,* *Department of Nuclear Engineering* University of Tennessee, Knoxville, TN
Dr. Lawrence Heilbronn	*Associate Professor,* *Department of Nuclear Engineering* University of Tennessee, Knoxville, TN
Dr. Ania Szynkiewicz	*Associate Professor,* *Department of Geology* University of Tennessee, Knoxville, TN
Dr. John D. Auxier II	*Adjunct Professor,* *Department of Nuclear Engineering* University of Tennessee, Knoxville, TN *First Line Manager,* *TA-55, Actinide Analytical Chemistry* Los Alamos National Laboratory, NM
Dr. Ning Xu	*Deputy Group Leader,* *Actinide Analytical Chemistry* Los Alamos National Laboratory, NM

Dedication:
TBD

Acknowledgement: TBD

Maik Lang

John D. Auxier II

Ning Xu

Ania Szynkiewicz

Lawrence Heilbronn

Dana Labotka

Beth Judge

Samuel Clegg

Anthony Faiia

Michael Koehler

John SEM

Miguel Crispello

Ryan Unger

Igor Gussev

Eric O'Quinn

Will Cureton

Raul Palomares

DOE Fellowship

And DHS funding CREDIT

Abstract: TBD

Overarching research question: ***Do nuclear reactions in surface environment lead to distinctive chemical and isotopic signatures that are not present in nature?*** Testable hypothesis: ***Nuclear processes will lead to distinctive chemical and isotopic patterns of partitioning because high-temperature processes under high radiation rarely occur in natural surface environment.***

Preface:

This research is largely split into the two main thrusts of nuclear forensics: pre-detonation studies and post-detonation studies. Each research focus pertains to drastically different physical systems, linked by a common chemical host – plutonium.

Chapters X-XX will discuss characterization of plutonium primarily in its metallic form, focusing on age, thermal history, and damage accumulation. They are a set of supporting studies…

Chapters XX-XXX detail the coupling of multivariate data analysis techniques to hand-held laser induced breakdown spectroscopy for on-site quantitative analysis of nuclear debris in a post-detonation scenario.

The aim of this research is to improve nuclear forensics capabilities, offering insight to rarely linked characterization methods (i.e. IRMS and Raman spectroscopy), in the scope of a plutonium-based nuclear weapon's life cycle.

Table of Contents:

List of Figures

Chapter 1

Introduction

Technical Applications

Brief history of nuclear weapons

Metallic Plutonium System

Technical background of Pu – crystal structure, alloying agents

Current Understanding of the Pu System

Temperature-Induced changes

Oxidation

Radiation-Induced changes

Damage Accumulation

Shortcomings of characterizing the system

There is a gap in scientific knowledge as to how nuclear reactions in surface environment lead to distinctive chemical and isotopic signatures that are not present in nature, especially for nuclear forensics purposes. The first thrust of this research is geared toward isolating time, temperature, and radiation damage as influencing variables on the oxidation of metallic SNM. Due to the exposure to high-temperature processes under high irradiation environments, it is expected that there will be distinctive chemical and isotopic patterns of partitioning in these materials.

Detonation-induced changes

The remainder of this dissertation focuses on the post-detonation scenario, in which case a Pu-based nuclear device has been detonated. In this case, the techniques previously mentioned which target surface effects are non-applicable to the metallic plutonium system. The system itself has completely transformed at this point through massive explosion dynamics subject to high levels of

radiation at temperatures between 5000-20,000 K, leaving behind melted glass debris. In order to properly characterize the Pu at this point in its life cycle, one must be able to accurately identify the composition of the melt glass which consists of Pu and its fission products, parts of the device infrastructure, as well as a host matrix comprised of the surrounding soil.

Explain more technical about the formation of the glass

Shortcomings of characterizing the system

Benchtop methods, etc.

Chapter 2

Pre-detonation Materials

Overview

Increased tension between nuclear weapon states, development of new and advanced weapons as well as the update and recycling of actinide material either previously archived or in the current dated stockpile are all pressing developments. The need for accurate analysis of actinide containing material both pre- and post-detonation is integral to maintaining national preparedness, safety, and security. In the following sections, the types of nuclear material targeted in this research are reviewed and emphasis is placed on where there exist deficits in analysis and characterization.

2.1 Literature Review

There is a critical need in nuclear forensics for a novel technique able to rapidly and effectively characterize intercepted special nuclear material (SNM). Some SNM exists in alloyed systems, such as PuGa, and present distinct signatures as they undergo aging[6,10,11]. The signatures that emerge include changes in electrical transport properties, structural defects due to self-irradiation, and surface oxide formation and growth. These alloys are also subject to elevated temperatures during fabrication, operation, and the decay of Pu-239[4]. Thus, high temperatures must be an integral part of aging studies as well as an understanding of damage accumulation from self-irradiation. Cu metal serves as an appropriate surrogate due to its face-centered cubic (FCC) crystal structure, which matches that of δ phase Pu. This phase of Pu is desirable due to its tough and malleable properties, but only possible when pure Pu is kept at high temperatures[12]. To keep the delta phase at room-temperature it must be alloyed with ~3wt% Ga (or another element such as Al) for it to resist transforming back to its stable alpha phase. However, the introduction of this

new alloying element renders simple decay laws unreliable. A new technique to determine the age of the material is then necessary to develop.

2.1.1 Cu as a surrogate for Pu

Cu as a surrogate for Pu works well beyond their shared crystal structure. They also undergo similar oxidation growth (Fig. 1). The increasing damage inflicted in Cu metal by ion irradiation and subsequent oxidation formation mimics the oxidation of PuGa systems.

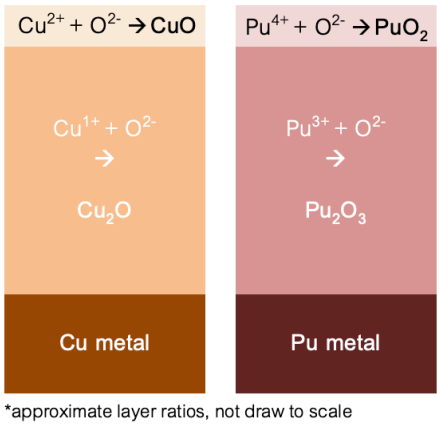

Figure 1: Visualized oxidation in dry air at 350°C for Cu (left) and Pu (right).

In elevated temperatures (350°C) and dry environments, a thicker initial layer of lower valence state Pu^{3+} (Pu_2O_3) and then a thinner higher valence state Pu^{4+} (PuO_2) forms on top as measured by XRD and XPS in a study by Haschke, *et al.*[13]. The ratios of these oxide species remain markedly similar to Cu (Cu_2O followed by CuO at temperatures above 200°C). This layering observed at 350°C indicates a change in mechanism observed through the break in the parabolic oxidation curve which is known to be caused by two different protective oxides in the Cu system[14]. Furthermore, at a temperature of 350°C with increasing damage, a lesser fraction of CuO is observed than without damage at the same temperature much like with Pu at elevated temperatures and increasing time scales (correlated to damage), there appears to be a lesser amount of PuO_2. This is due to the further reduction of PuO_2 into Pu_2O_3. Stakebake validated that the lesser oxides

of Pu form above 350°C, and that the increase in oxidation time in the PuGa systems causes a similar trend in O gain as seen in the Cu oxide system (Fig. 2)[14].

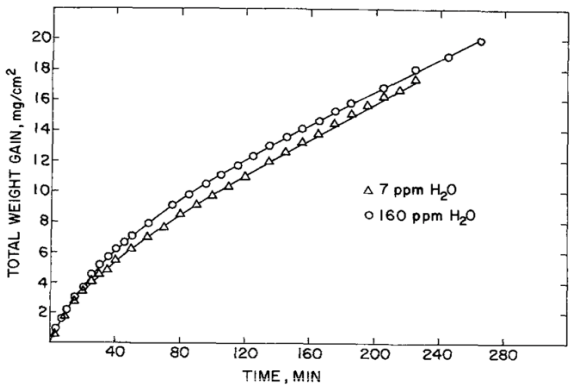

Figure 2: The effect of low-level moisture concentrations on the oxidation of plutonium-3.3 a/o gallium in air at 350°C[14]

In summary, as ∂ phase Pu and Cu oxidize, they undergo similar O adsorption, oxide phase growth, and growth mechanisms with increasing temperature and time, in similar environments. Therefore, if the same characterization methods are applied to Pu oxide surface as proposed on irradiated Cu oxide surfaces, we should be able to draw a convincing comparison.

2.1.2 Aging: Oxidation

Thermal aging is one of the methods commonly used to simulate natural aging in materials beyond laboratory time frames. The theory is that the basic reaction rate equation includes dependencies for time and temperature, and thus, is able to be manipulated to produce the results often seen in long time-scales in shorter periods by increasing the temperature. Sometimes it is used in a cyclical process until the desired effects are produced. Thermal aging is routinely applied to a variety of materials including both metals and polymers[15]. Wright completed a study on Inconel 617, a Ni-Cr-Co-Mo alloy, where thermal aging is applied to examine oxide grain growth with increasing time and temperature as well as the alloy's performance under stress loading[16]. Wang observed

thermal aging effects on thin films of tin upon a Cu substrate where the oxide growth was measured as thickening in air, and the specie of oxides that formed was dependent on temperature[17,18].

These types of experiments are plentiful, providing a rich background on the thermal aging and oxidation of metals and are aligned to what is proposed in the sections below. It is the goal of these aging experiments to explore both time- and temperature-dependent effects, as well as those induced by irradiation at a fixed time and temperature.

In good company to thermal aging experiments is literature on the specific mechanisms for oxidation growth on Cu metal. O molecules adsorb and dissociate as ions, borrowing electrons from the Cu metal, on the surface to form a string of Cu-O-Cu-O[19]. The formation of O ions simultaneously creates cation vacancies, thus inducing an electrically conductive gradient through which Cu ions (Cu^{+1}) may travel to the oxide interface (Cu_2O/O_2)[20].

When the O molecules adsorb on the metal, they do so at a concentration influenced by the temperature and atmosphere. Oxidation of metal surfaces is rate limited by diffusion through the oxide layer, which increases strongly with increasing temperature. However, the oxides in the irradiated Cu study outlined below were formed at one fixed temperature and one fixed time at the same atmospheric O partial pressure, which virtually eliminates the possibility of varying diffusion rates. This being said, the differences in oxide observed between these samples come from the surface morphology as damaged by ion irradiation, and that subsequent effect on O adsorption at the surface. Diffusion of along grain boundaries of Cu_2O is attributed as the mechanism for oxidation in the temperature regime chosen for all studies (200°C - 550°C), so it is expected to see the oxide growth affected by the size of the Cu_2O crystals[21].

2.1.3 Damage: Irradiation

When radioactive Pu decays, it does so by splitting into a U atom and an α particle. While the α particle creates helium bubbles, the recoil energy off the U atom sometimes displaces Pu atoms from their original lattice sites, leaving vacancies which sometimes become mobile and form clusters (voids)[13]. The creation of both He bubbles and voids cause overall swelling in the lattice. This is the result for almost every metallic compound subject to high levels of radiation at a fraction of 1/3 its melting temperature[13].

In order to simulate SNM evolution over a life-time of radiation exposure, ion irradiation is often employed. This induces damage effects correlating to fission products, critical to our understanding of defect accumulation in SNM. In many studies, surrogates are used as detailed above to test techniques for a cheaper cost - specifically those in the FCC family when the SNM of interest is PuGa alloys. At the onset of an ion bombarding a material, a collision cascade is formed where a high concentration point defects are produced close together. The majority of these defects will spontaneously recombine or agglomerate where the defects will either be resolved or clustered, respectively. If a defect produced from the original primary knock on atom (PKA) lands outside of the spontaneous recombination radius, they may become freely migrating vacancies or interstitials. Understanding how these defects form and mobilize allow one to predict material property transformations.

The variety of defects induced through irradiation often make it difficult to quantify damage specifically. Often displacements per atom (dpa) is employed as a way to compare across differing types of irradiation studies (ion, neutron, electron, etc.) and defects produced. The damage can be approximated using James Ziegler's program SRIM (**S**topping and **R**ange of **I**ons in **M**atter). SRIM is a collection of software packages that calculate many features of the transport of ions in matter. It uses Monte Carlo techniques to model ion beam interactions in targets. It calculates

damage energies, full cascades, and has graphics representations of ion paths so one can get qualitative information about where the most ion damage is occurring. This specific part of the program is called TRIM (**Tr**ansport of **I**ons in **M**atter). These codes allow one to enter in a variety of experimental parameters and calculate results including but not limited to penetration depth and ion energy loss (based on target material stopping powers). By choosing parameters corresponding to Pu self-irradiation defect accumulation rate of 0.1 dpa per year, similar damage can be induced in other FCC metals such as Cu through heavy ion irradiation[23]. Ion irradiation can be used to achieve high displacement rates in a short duration of time. This means, to simulate for damage accumulated in Pu in 50, 100, and 150 years, there needs to be 5, 10, and 15 dpa worth of damage inducted in the Cu. The TRIM code cannot directly calculate dpa, but there is a method due to Stoller et al. that allows for an accurate damage calculation using TRIM utilizing the "quick" Kinchin-Pease model to compute the damage. Stoller et al. found this method to give a better approximation for the damage than the standard TRIM calculation[24]. The method includes setting the lattice and binding energies to zero. The Kinchin-Pease model gives the number of Frenkel pairs produced per ion as:

Eq. 2 $$\nu = 0.8T_{dam}(E_{PKA})/2E_d$$

the average displacement per ion (dpi) per length is then given by ν/l, where l is the effective range of the ions. We are using the average method to ensure that the average damage in the irradiated layer is 5, 10, or 15 dpa. With the dpi in hand, the required fluence Φ is then:

Eq. 3 $$\Phi = \frac{dpa}{dpi}\Omega$$

where Ω is the atomic density. Finally, the time for irradiation may be obtained from:

Eq. 4 $$t = \frac{\Phi}{\Omega}$$

where φ is the flux of the beam.

Experimental Shortcomings for Characterizing Pre-detonation Material

The leading analysis techniques for pre-detonation material include a variety of radiochronometry methods. Utilizing actinide ratios such as $^{235}U/^{239}Pu$, etc. depending on target material provides information into compositional history of the radioactive elements[25]. These studies are often validated on Standard Reference Material (SRM). The most popular methods fall into either decay counting such as gamma or alpha spectrometry or mass counting methods such as Secondary Ion Mass Spectrometry (SIMS), Thermal Ionization Mass Spectrometry (TIMS), or Inductively Coupled Plasma – Mass Spectrometry (ICP-MS)[26]. However, the decay counting techniques require larger sample masses and the mass counting techniques are largely destructive – both of which are to be minimized in the following proposed research methods.

2.2 Experimental Methodology for Material Preparation of Cu metal

2.2.1 Electrochemical Polishing

Electrochemical polishing is used in many industries as a way to gently clean the surface of metals[38]. A clean, reproducible surface was key to the aging experiments requiring a careful and reproducible polishing procedure. By applying a current through a metal within a solution medium, the outermost layer of the Cu squares is removed through a process similar to reverse hydrolysis. In this research, the solution is a mixture of deionized water (DI) with 2 wt% KOH. A pair of

stainless steel curved tweezers re placed into the solution on the lip of the beaker to serve as the anode (AT). Another set of tweezers are then tapped to a non-conducting rod and used as the cathode (CT). The voltage source (Lavolta BPS305 Variable Linear DC Power Supply) is set parallel to the magnetic stirring plate, and the negative and positive alligator clips is attached to the base of the anode and cathode tweezers, respectively. A small beaker of pure deionized water is placed within the fume hood as well as for sample rinsing between polishing segments. The first sample is pinched by the CT and held in place by clamping the alligator clip mid-way down the tweezers. It is crucial to ensure that the tweezers did not cover a substantial portion of the Cu square surface area, therefore, a priority should be to pinch as close to the sample edge as possible. Holding the CT at the non-conducting end, the following steps are taken[39]:

1. A 17.5 V source is applied to the stirred solution while the Cu square is submerged completely and parallel to the current flow of the liquid.
2. The sample is left for 20 seconds, taken out of solution and dipped into DI for quick rinse.
3. The voltage is increased to 25 V and step 2 is repeated.
4. The voltage is increased to 30 V and allowed to dry on a clean surface.
5. Steps 1-4 are repeated until all samples were polished; the 2 wt% KOH solution should be changed after every 4-5 samples to avoid deposition of impurities gathered from the solution back onto the sample surface.

2.2.3 Thermal Aging

Thermal acceleration is one of the methods commonly used to simulate natural aging in materials beyond laboratory time frames. Often it is used in a cyclical process until the desired effects are produced and higher temperatures are employed to reduce the treatment time. This process is routinely applied to a variety of materials including both metals and polymers[15]. In this research,

the oxidation of Cu is to be investigated in terms of characteristic signatures that are induced by exposure to atmospheric air. Once the polished Cu samples from **4.1.1** are dry, they are placed atop an Al_2O_3 (alumina) circular disc and inserted into the furnace for heating. Alumina was chosen as an inert high-temperature tolerant ceramic to minimize the possibility of either reaction or O diffusion from the substrate to the Cu matrix. The ramp-up rate is set 10 °C per minute with a dwell time varying for the appropriate experiment as shown in Table 4. There will be no ramp-down rate set and the furnace should be allowed to cool while switched off until the inside temperature reached below 100 °C. It is important to note that each sample is to be run individually and that no interruption in heating regime occurs.

Table 4. Oxidation parameters for both temperature–dependent and time-dependent aging experiments.

	Temperature	Time
Temperature-dependent Series	250 °C	1 hour
	300 °C	1 hour
	350 °C	1 hour
	400 °C	1 hour
Time-dependent Series	350 °C	1.5 hours
	350 °C	2 hours
	350 °C	2.5 hours
	350 °C	3 hours
	350 °C	3.5 hours

The samples are then removed with metal tongs and allowed to further cool to room temperature before being placed into a container for further analysis. The inner atmosphere of the furnace itself

is not controlled to any set humidity in order to simulate realistic conditions of natural oxidation occurring during exposure to air. The thermal-aging experiments will be performed in 3 independent runs: (*i*) one set of polished, oxidized Cu square samples for both temperature- and time-dependent experiments. (*ii*) and (*iii*) two separate sets of Cu square samples for validation of IRMS measurements of the temperature-dependent experiments. All three runs are used for the temperature-dependent series to assess data reproducibility of O isotope fractionation in the Cu oxide phases. NaF will be added to Run 3 in order to assess whether the reagent had an effect on combustion which ensures that the entire sample was analyzed. The post-irradiation thermal-aging experiments will be performed as one run with all experimental parameters remaining the same except for a fixed dwell time of one hour at 350°C for all samples.

2.2.4 Ion Irradiation

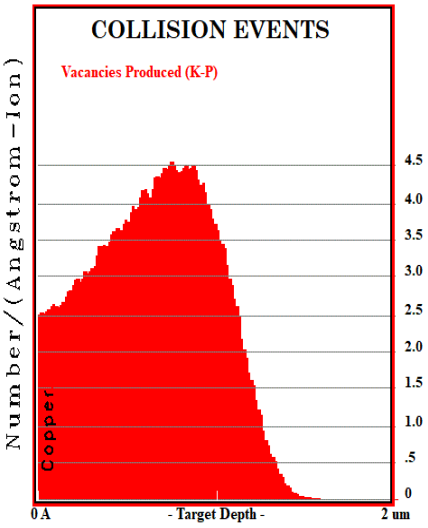

Figure 4: Relative damage versus distance (TRIM).

Over time, decay of Pu in PuGa alloys creates defect tracks, which affect the materials structure and thus provides a traceable physical property[6]. It is the goal of this study to mimic this environment through ion irradiation in a surrogate metal. Three 6×6 mm Cu squares that are 0.8 mm thick are to be irradiated with 10 MeV Au^{3+} ions at a particle flux of 1×10^{12} ions/cm^2/s. The

irradiations will be performed at the Ion Beam Materials (IBML) accelerator at the University of Tennessee. For the calculations in SRIM, 10 MeV Au^{3+} ions at the aforementioned flux of 10^{12} ions/cm^2/sec is input with the target as pure Cu metal at a density of 8.92 g/cm^3 to produce estimated damage shown in Tables 5-7 below. Correlating to the 0.1 dpa/year naturally produced in Pu through self-irradiation, it is the aim of this study to track 50, 100, and 150 years of damage (5, 10, and 15 dpa respectively). A MATLAB code was created that takes the SRIM output together with the beam input parameters and gives an irradiation time. The dpa value calculated using [40] is to be interpreted as an average dpa over the total irradiated range, which one can see in Figure 5. For this reason, we used Au ions, which have a flatter damage profile when compared to lighter ions such as Ni. Each sample was prepared individually so as to not expose it to the heat for any longer than necessary. The irradiation is estimated to take a total of 14 hours with the beam setup and stabilization. The samples will be irradiated at a temperature of 200°C corresponding to approximately $0.35T_M$ of Cu. The difference in defect recovery at room temperature vs. 200 °C is significant but is at this temperature that microstructure evolution is most readily observed. From our preliminary calculations, we are estimated a beam current of 250 nA.

Table 5. Input parameters for TRIM calculations and irradiation parameters

List of irradiation conditions			
Sample	A	B	C
Ion beam	Au^{3+}	Au^{3+}	Au^{3+}
Total dose (dpa)	5	10	15
Fluence (ions/cm^2/s)	1.63×10^{15}	3.26×10^{15}	4.89×10^{15}
Time (min)	27	54	82
Temperature (°C)	200	200	200
Input parameters for TRIM calculations		Relevant Output parameters from TRIM calculations	
Ion species	Au^{3+}	Ion energy loss	0.08%
Ion energy (MeV)	10	Atom energy loss	32.62%

Target width (mm)	0.8	*losses due to phonons	
Target density (g/cm^3)	8.92		
Target composition	Cu		
Displacement energy [50] (eV)	30		
Surface and binding energies (eV)	0		
Number of ions	100,000		

2.3 Analysis Techniques

2.3.1 Isotope Ratio Mass Spectrometry (IRMS)

Over time, materials experience isotopic fractionation, or the active separation of isotopes of a single element, due to chemical, physical, and biological influences with two major influences being temperature and pressure. This creates distinct signatures which are able to discern origin, history, age, etc. of a given material. Isotope Ratio Mass Spectrometers have been popular for use in origin studies in geochemistry, archaeology, and forensic studies due to their ability to precisely and accurately measure natural stable isotopic abundance of light elements (H, C, N, O, S)[41, 42]. Specifically, in explosives, IRMS has proved to be a useful tool for differentiating among isotopes of ammonium nitrate and certain plastics in trace amounts[43,44]. In the field of nuclear studies, IRMS has recently been used for the preparation and validation of Pu age dating materials[45]. Namely, for evidence towards material accountancy declarations, as well as origin of material. There are several mechanisms contributing to the effectiveness of this technique in such high-stake studies. The rapid results inherent in most spectroscopic and spectrometric techniques is one of the most attractive qualities of IRMS.

Initially, the sample is injected into the inlet of the spectrometer where it is vaporized and transferred to a column with use of helium as a carrier gas. It is then allowed to react with both the carrier gas and inner coating of the column to separate the compounds desired for measurement, sweeping the resultant mixture into a combustion chamber where they are oxidatively combusted

into a simple gas, such as CO, CO_2, H_2, of N_2. Any water is removed from the system by passing this stream of gas through a selectively permeable tube and then sending it through a basic electron ionization device to create ions[46]. The gas ions are further guided along the spectrometer by a bending magnet (magnetic sector analyzer), separating the ions based on mass through this process, and collides the separated stream of ions with a series of faraday cups, lined up to match each mass of isotope. IRMS measures the continuous flow of these ions. By measuring the O isotope fractionation in Cu oxide layer grown of the pristine thermal aging experiments at each time and temperature, this technique allows insight to the probable relationship between fractionation and specific oxide specie formation.

2.3.2 Raman Spectroscopy

In Raman measurements, a beam of monochromatic light is directed at the sample surface, and its electromagnetic field interacts with the electrons of the sample, causing a change in polarizability. These electrons typically elastically scatter the light (Rayleigh scattering), but a fraction of electrons is shifted (Stokes and Anti-Stokes scattering). The change of wavelength in the emitted light is characteristic of a specific element or compound. The light directed on the sample causes a temporary deformation in the molecular structure through electromagnetic interference and causes that molecule to vibrate at a characteristic frequency. The pathway that the molecule scatters the excess energy depends on the initial state of the molecule. The elastic scattering is unideal for Raman measurements, and oftentimes is blocked by the use of special apertures so that the weaker signals from inelastic scattering can be more clearly recorded[47]. Raman spectroscopy can provide insight into local bonding structure as well as fraction of crystal species in the sample derived from peak analysis. In current studies of nuclear forensics, Raman has been used to characterize uranium tetrafluoride (UF4)[48], seized uranium-containing material[49], and zirconium-

uranium alloys from the Chernobyl nuclear power plant[50]. Relevant to the study in this proposal, it has been noted in UO_2 studies[51], and temperature dependence of its oxide formation[52].

A Mirco-Raman Horiba LabRAM HR Evolution will be utilized in this research to acquire spectra of all time-, temperature-, and irradiation-dependent series of oxidized Cu samples. A green laser of 532 nm will be the excitation source. The spectra will be recorded with a liquid nitrogen-cooled charge coupled device detector. Previous to any measurement, the machine would be calibrated with a Si sample to ensure all components are functioning and would produce reliable spectra. A 50x magnification lens will be used to focus on the oxide layer surface in atmospheric air with a laser power of 1%. This low power was selected to avoid heating and potentially further oxidizing the samples. The Raman spectrometer is operated in confocal mode with a beam-spot size of ~2 μm. All spectra will be recorded by two accumulations of 60 second measurements for each sample. The software package Lab Spec 6, is employed to control all parameters, focus the lens, and display the collected spectra.

2.3.3 X-ray Diffraction

Pre-detonation material is often in need of analysis that does not require destruction of the sample. The measurement of small amounts of powder samples can be accomplished through synchrotron X-rays. Adopted from the small sample volumes that are characteristic of high-pressure experimental procedures, microscopic sample chambers are prepared in a thin molybdenum foil by drilling several holes with a diameter of ~100 μm. The foil thickness was 50 μm. Sample chambers are cleaned in an ultrasonic bath with acetone, and the sample powder is placed over the holes and pressed between two steel die-pieces in a hydraulic laboratory press. Synchrotron X-ray analysis are performed at the Advanced Photon Source (APS) of Argonne National Laboratory using sector 16 (HPCAT, High-Pressure *Collaborative Access Team*). A highly-focused X-ray

beam (spot size 25 μm) is used to study the small amount of Cu oxide sample. The structure is investigated in transmission mode by means of angle-dispersive micro X-ray diffraction (XRD). Grazing incident X-ray Diffraction (GIXRD) will also be utilized in this research to gain structural information on the surface of irradiated Cu metal in order to capture the thin layer of damage induced through ion irradiation. XRD was performed at the Joint Institute for Advanced Materials (JIAM) Diffraction Facility, located at the University of Tennessee, Knoxville.

Chapter 3

Time- and temperature-dependent signatures of Cu oxides through O isotope fractionation

3.1 Abstract

3.2 Introduction

3.3 Experimental Setup

3.4 Results

3.4.1 Raman Spectroscopy

3.4.2 Isotope Ratio Mass Spectrometry

3.5 Discussion

Did research answer *Objective I: Understanding time- and temperature-dependent signatures of SNM (pre-detonation) through O isotope fractionation?* Research objective I involves studies that are structured to answer the following: How accurate of a tracer are O isotopes for the oxidation of metallic manufactured materials? Do O isotopes have preferential bias to bond in only certain oxide species (crystal structure)? Many recent studies have focused on the development of unique and minimally destructive analysis techniques for chronicling metallic material, specifically special nuclear material (SNM). Isotopic fractionation is known to be influenced by kinetic changes such as those in temperature and pressure. Studies designed to accomplish research objective I will provide experimental data on O isotope ratios in thermally aged Cu oxides isolating both time and temperature as observed variables. These studies will be paired with structural data of the Cu oxides obtained through Raman spectroscopy to understand if there is a distinct trend between the fractionation of O species and formation of Cu oxide species.

Chapter 4

Structural modification of Cu metal and Cu oxide through ion irradiation

4.1 Abstract

4.2 Introduction

4.3 Experimental Setup

4.4 Results

4.4.1 Scanning electron microscopy

4.4.2 X-ray Diffraction

4.4.3 Raman Spectroscopy

4.5 Discussion

Did research answer *Objective II: Determining the effects of ion irradiation on SNM and how damage affects oxidation over time (pre-detonation)?* Research objective II involves studies that are structured to answer the following: What effect is made on the crystal structure of ion irradiated Cu metal and how does that translate to the thermally induced oxide layer? Studies of irradiation in metallic oxides typically involve in situ measurements of oxidation growth or inducing damage on already formed metallic oxides. The effects of irradiation damage on metal and the influence it has on the formation of oxides at high temperature (350°C) has not been a focus in the radiation damage community. Pu metal and its alloys are often heated in a variety of manufacturing procedures. The exposure to high temperatures triggers the oxidation process. The exploitation of the oxide layer could serve as a key signature in identifying thermal histories of the material as well as radiation history (type of damage correlating to existence of certain radioactive fission products) if this research shows that the defects produced in the metal remain as a signature in the oxide layer. To accomplish this goal, synchrotron X-ray diffraction will elucidate any structural

changes with high precision from the transition from metal to oxide. Raman Spectroscopy will be utilized in order to compare across studies from research objective 3.1 and characterize the oxide species with increasing dose primarily.

Chapter 5

Pre-detonation Materials

Overview

Nuclear debris, resultant in the event of a nuclear detonation, undergoes a complex formation process. At time zero, the nuclear device is deployed. In a short time following, this device detonates producing a mass ejection of both neutrons and x-rays, pushing out a fireball and wall of immense pressure. When the pressure and shock wave connect with the ground, part is reverberated upward after impact sending with it a large amount of earth with it. The temperature in this cloud of mixed debris is anywhere from 5000 to 20000 K, melting virtually all elements and mixing them in a turbulent, radioactive plume. When this mixture cools, which takes place over multiple time scales, it settles in the form of bead and tear-drop shaped glasses. The task once this process finalizes is to accurately identify from those glasses what type of device was used and where did the material originate from[27].

5.1 Literature Review

Insert here

5.1.1 Nuclear Underground Engineered Test Surrogates (NUGETS)

In order to obtain accurate measurements on the composition of melt glass, it is often sent back to a laboratory for measurement through a table top mass spectrometer such as an Inductively Coupled Plasma Mass Spectrometer (ICP-MS). This process yields reliable results but sacrifices precious time. Some decay products have half-lives on the order of minutes which would not be detected by the time the sample is transported back to a proper facility[27]. The focus in post-detonation nuclear forensics is currently to develop novel techniques for on-site characterization. Over the past decade, great strides have been made in the replication of this glassy fallout for use

in pinning down advanced characterization methods[28]. Boone, Auxier, Seybert, Molgaard, etc. have formulated a method for reproducing this slurry dependent on location of detonation. They have been successful at producing synthetic glasses for trinity site[29], New York, New York and Houston, Texas[30] as well as glasses representative of underground detonation at the Nevada test site[31]. In addition, there have been preliminary studies focused on urban/marine environments[32].

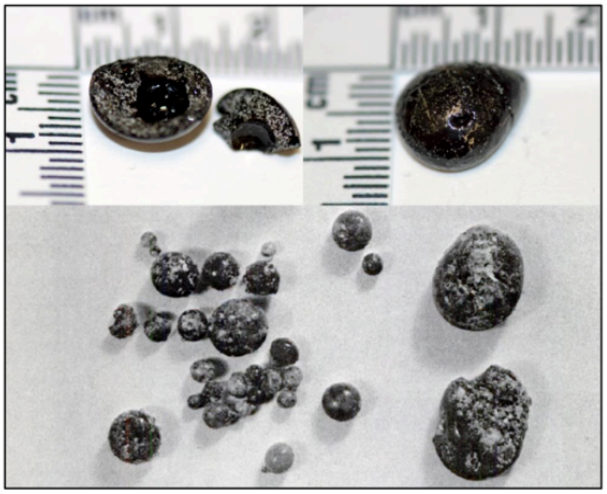

Figure 3: NV1C Sample bottom side (top left) and reflective side (top right) as compared to underground nuclear explosive melt debris (U-NEMD).

Compound	NV1X (wt-%)
SiO_2	71.27
Al_2O_3	14.36
CaO	3.72
Na_2O	1.178
Fe_2O_3	2.48
K_2O	4.51
MgO	0.75
P_2O_5	0.119
TiO_2	0.34
MnO	0.07

Table 1. List of NUGET NV1X samples compositions in weight percent.

This study utilizes the Nuclear Underground Engineered Test Surrogates (NUGETS, NV1X series Fig. 3). Composition of these melt glasses are found in Table 1. For explicit methodology on the mathematical formulation of the synthesized components the reader should refer to Boone[31]. The NV1X series were formed through firing in a furnace. NV1A and NV1B were fired below the liquidus point at 1500°C for 30 minutes while NV1C was fired at 1600°C for 35 minutes and NV1D at 1570°C for 30 minutes. This is to simulate the variety of thermal exposure to the soil and

replicate melt glass in different locations. Specifically, for underground nuclear melt glass, the elemental composition is majorly constrained to the host geochemistry but will also include elements representative of the device components, activation products, and fission products dependent on the type of fuel[31].

In pursuit of characterizing these materials, inductively coupled plasma-mass spectrometry (ICP-MS) is often employed to obtain high fidelity measurements of specific elements and their concentrations. In reality, when conducting these measurements, the user is really measuring isotopes while assuming their natural abundances. ICP-MS requires the sample to be in liquid form, which often involves a digestion process accomplished by the use of an acid. It is more difficult to measure elements that tend to form negative ions such as Cl, I, and F due to their ionization energy. This is one limitation of using ICP-MS – it is capable of detecting any element, but in order to get the elements through the instrument relies heavily on their ability and ease of ionization. Other limitations of ICP-MS come in the form of interferences, which can either be related to the environment or the analyte and spectrometric processes themselves. These involve isobaric, polyatomic/adduct ion, and doubly charged ion interferences. It should be noted that sending samples from the site back to an equipped laboratory for non-destructive and destructive analysis (NDA and DA, respectively) is still an incredibly critical step of nuclear forensics, integrated to provide unparalleled information on these samples. However, the scope of this research on nuclear melt glass will focuses on the first line of analysis and identification.

5.1.2 Environmental Standards

Utilizing standards as a means of comparison for the chemical characterization techniques proposed in this document is critical for validation of results. Particularly, when studying synthesized materials that were not manufactured by an accredited company such as the

aforementioned NUGETS, comparison to a known composition is mandatory. In the procedures outlined below, NUGETS samples will be compared primarily to the National Institute of Standards and Technology (NIST) Standard Reference Material (SRM) 610 standard[33]. This standard has a known composition (Table 2) and has been used in previous studies as an acceptable comparison for nuclear melt glass due to its trace amounts of uranium and other fission products[34,35].

Compound	NIST 610 (wt-%)
SiO_2	72
Al_2O_3	2
CaO	12
Na_2O	14
Trace Element	
Fe	0.0458
Mn	0.0457
K	0.0461
Ti	0.0437

Table 2. Composition of NIST 610 glass standard

In addition to this standard, in the formulation of the Partial Least Squares Regression (PLSR) code detailed in the sections below, a number of standards between 20-30 will be used (Table 3). These will be from the same source of those utilized for the calibration of the ChemCam on Mars[36,37]**.** These samples contain at least 5 compositions higher and lower than the specified NUGET compositions (except for K_2O, which is difficult to find standards with high concentrations).

Table 3. Geological Standards utilized for analytical comparison and model formation.

Sample	SiO_2	TiO_2	Al_2O_3	Fe_2O_3T	MnO	MgO	CaO	Na_2O	K_2O	P_2O_5
AGV2	59.30	1.05	16.91	6.69	0.10	1.79	5.20	4.19	2.88	0.48
BCR2	54.10	2.26	13.50	13.80	0.20	3.59	7.12	3.16	1.79	0.35
BEN	38.20	2.61	10.07	12.90	0.20	13.15	13.87	3.18	1.39	1.05

BHVO2	49.90	2.73	13.50	12.30	0.17	7.23	11.40	2.22	0.52	0.27
BIR1	47.70	0.97	15.40	11.33	0.18	9.70	13.40	1.81	0.03	0.03
BK2	58.83	1.94	14.77	8.78	0.19	2.82	4.64	3.35	3.99	0.71
BT2	48.57	1.52	16.46	11.09	0.15	6.42	7.92	4.48	1.28	0.44
GBW07103	72.83	0.29	13.40	2.14	0.06	0.42	1.55	3.13	5.01	0.09
GBW07113	72.78	0.30	12.96	3.21	0.14	0.16	0.59	2.57	5.43	0.05
GBW07311	76.26	0.35	10.37	4.78	0.32	0.62	0.47	0.46	3.27	0.06
GBW07312	77.29	0.25	9.30	6.20	0.18	0.47	1.16	0.44	2.91	0.05
JR1	75.41	0.10	12.89	0.89	0.10	0.09	0.63	4.10	4.41	0.02
UNSZK	74.38	0.04	14.19	1.75	0.03	0.07	0.43	4.50	4.06	-
GBW07104	60.62	0.52	16.17	4.90	0.08	1.72	5.20	3.86	1.89	0.24
GBW07114	0.58	0.02	0.09	0.21	0.01	21.64	30.00	0.03	0.04	0.01
GBW07217A	0.95	-	0.29	0.38	0.06	20.91	30.67	0.02	0.00	0.00
GBW07110	63.06	0.80	16.10	4.72	0.09	0.84	2.47	3.06	5.17	0.36
NAU2	48.70	0.60	4.53	31.76	0.02	0.77	1.96	0.70	0.13	-
JA2	56.42	0.66	15.41	6.26	0.11	7.60	6.29	3.11	1.80	0.15
JA3	62.26	0.68	15.57	6.59	0.11	3.65	6.28	3.17	1.41	0.11
SWY1	62.90	0.09	19.60	3.71	0.01	3.05	1.68	1.53	0.53	0.05
JB1B	51.11	1.26	14.38	9.01	0.15	8.14	9.60	2.63	1.32	0.26
JB2	53.20	1.19	14.64	14.34	0.20	4.66	9.89	2.03	0.42	0.10
JB3	51.04	1.45	16.89	11.88	0.16	5.20	9.86	2.82	0.78	0.29
JA1	63.97	0.85	15.22	7.01	0.16	1.57	5.70	3.84	0.76	0.17
GUWGNA	71.47	0.02	14.70	5.92	0.17	0.03	0.62	0.08	2.63	0.00

Experimental Shortcomings for Characterizing Pre-detonation Material

5.2 Experimental Methodology

5.2.1 NUGETS synthesis

Insert here

5.2.2 Ammonium Biflouride Digestion

The most sample destructive component in this research is the use of ammonium biflouride (ABF) for digestion. However, this is only a technique used to validate the experiments outlined in 4.7. This is a chemical digestion technique and to be used on material that has completed all other characterization techniques, as the process irreversibly destructs the sample. Following Hubley, *et*

al. [34] procedure, approximately 20 mg of NV1X series of NUGETS are loaded into a Savillex PFA 15 mL conical test tube. Solid ABF is added so that a 7:1 ABF to sample ratio was maintained and then the samples are heated for 30 minutes in an Al hot block at 230°C. A volume of 2 mL of HNO_3 is then added to each test tube which is then heated for 1 hour at 160°C in the Al hot block. The aqueous samples are transferred to a PTFE beaker and rinsed with 18.3 MΩ high purity water then taken to near-dryness on a hot plate. The residue is dissolved in 2 mL of 8 M HNO_3 and transferred to a 15 mL Falcon test tube. The solution is then diluted to 10 mL with 18.3 MΩ high purity water. Rigorous studies in C-AAC proved that the concentration of the nitric acid during the sample heating does not have a large effect on the elemental recoveries of the NIST 610 glass[34]. Performing this digestion allows for a fast preparation and prevents the necessity of highly hazardous chemicals such as hydrofluoric acid. The possible recovery issues of this technique include Ca and Mg having a tendency to precipitate with F. Si will have poor recovery due to the reaction with ABF generating SiF_4 which will volatize off as a gas.

5.3 Analysis Techniques

5.3.2 Inductively Coupled Plasma – Optical Emission Spectroscopy (ICP-OES)

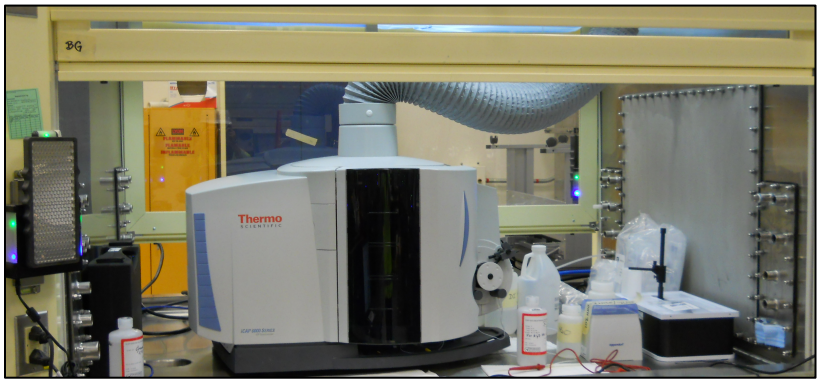

Figure 6: Image of Inductively Coupled Plasma-Optical Emission Spectrometer used in this study.

Upon complete digestion, the NV1X series of NUGETS are measured through and ICP-OES to obtain high fidelity measurements of specific elements and their concentrations (Fig. 6). The

solution from **4.6** is pumped through a peristaltic pump into a nebulizer to generate aerosol in the spray chamber, where approximately 10% of the analyte is actually transferred - the rest is drained due to the particle size being too large. Once in the spray chamber, the analyte is flushed through with argon gas, which both carries the analyte and is itself vaporized into a plasma by the ICP torch. The ion source for an ICP-OES, is a high temperature argon plasma coupled with a nebulized inlet spray. The discharge temperature for this is between 6000 -10,000 K, producing mostly positive ions[53]. When the plasma cools, the electrons drop back down to ground level energy and emit light of the characteristic wavelength that is compared with a calibration plot to give the concentration for that element in the sample[53].

5.3.3 Handheld Laser Induced Breakdown Spectroscopy (HHLIBS)

Laser Induced Breakdown Spectroscopy creates a laser induced plasma as the ion source for measurement. More specifically, it uses a pulsed laser to ablate the surface of a material into a plasma of ions, molecules, atoms, and particles[54]. LIBS is a primary technique for direct chemical analysis of solid samples and has a large following in the community of single particle analysis, and uranium isotope analysis[55,56]. One huge benefit to LIBS is that it can be performed in ambient conditions, meaning it does not require the use of utilities such as a vacuum pump. This also allows the device to be miniaturized and easily transported for use in field applications. Hand-held LIBS gained popularity due to its portability, quickness of results, and simplicity. There is the possibility of increased background noise dependent on the deployed environment. Therefore, it is important to note that this technique should be used in situations where onsite analysis is critical, and that removing the sample would either cause damage to the sample or create a hazardous environment for the analyst. The SciAps Z300 LIBS instrument will run in Element Pro mode, an uncalibrated mode, which formulates the relative abundances of elements within the sample as compared to one

another. This is a non-traditional approach in LIBS measurements as normally, the use of standards with the appropriate matrix is critical to interpretation of spectra. However, the investigator is not going to have a reference material to calibrate to if the sample and its constituents are unknown. The fundamentals of interpreting this type of spectra is relatively new, and because the mode is not meant to be quantitative, developing a method to retrieve useful information from the peaks is crucial if this technique is to be considered for nuclear forensic applications.

For Example:

NV1C	Element	Relative Abundance	Lines	Likelihood
	Ca	36.5	100	151
	Al	18.1	71.4	187
	Ti	8.39	84.6	72.6
	Na	7.76	100	93.6
	Si	7.35	100	64.7
	Tl	4.29	50	0.456
	Mg	3.8	90.9	47.7
	Ag	2.88	60	7.38
	Fe	2.58	92.3	45.4
	K	2.45	50	43.1
	Mn	2.25	65.2	22.2
	Rb	1.37	50	3.01
	C	0.568	100	1.97
	Sr	0.485	50	4.26
	Pd	0.373	42.9	3.27
	Li	0.352	100	0.707
	Cs	0.271	50	2.38
	H	0.157	50	1.38

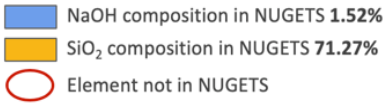

Figure 7: Example output from HHLIBS SciAps internal program. Highlighted and circled elements are indicated by image legend.

The algorithm identifies the major peaks in a spectrum, matches them to the list in the LIBSLINES, and reports the major elements present if a certain fraction of peaks is present (>50% of all peaks listed) (Fig. 7). The relative abundance (RA) value is proportional to the size of that element's peak versus all other peaks seen in the spectrum, and the RA values are normalized to 100. This type of measurement is a crude, qualitative measure of what major elements are present, and roughly how large their peaks are. The line percent is a ratio comparing the number of lines that

are detected in the spectra to the number of lines in the found in the library for an element and the likelihood rating uses this line percent to rate how likely it is that the element is actually present in the sample. While the option to tailor the internal libs line list is available to obtain higher confidence of relative abundances, it is not at the level of accuracy needed for nuclear forensic analysis. Therefore, it is crucial to further process the data through external means such as multivariate data analysis (MVDA).

5.3.4 Multivariate Data Analysis: Partial Least Squares Regression (MVA: PLSR)

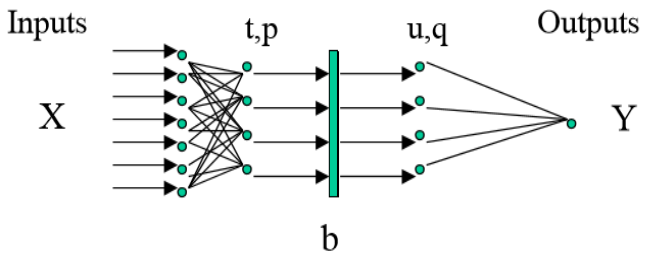

Figure 8: Diagram of partial least squares regression matrix transformations[57].

Partial Least Squares (PLS) Regression involves vectorization of input and output data, as well as a common inner transformation linking the two (Fig. 8). This technique is helpful for data sets in which a predictive model is needed. It projects an objective transformation of the data to determine covariance and ultimately create a linear model that effectively relates the input and output data. A model is usually built to optimize predictive efficiency by selecting the number of latent variables required to compute an accurate new observation. The method of comparing across models will assess the RSME or the root mean squared error. This is a universal way to compare each model to determine the approach that performs the highest and used as the figure of merit in the discussion. It considers the predicted values of the model as compared to the actual values and assigns an error correlating to how accurate the given model performs.

PLS considers the input and output variables as well as an inner transformation in the complete algorithm used. The inputs, outputs, and inner transform are vectored in order to find the latent variables. These latent variables are found from an iterative process of using the largest eigenvector of between the given input and output and using the scores to project back on the original matrix resulting in the loadings. Each successive iteration will have less predictive power because the highest eigenvector is used in the first iteration, so an optimal number of eigenvectors was selected through cross-validation. This method multiplies the test inputs by the inner transform vectors, which are correlated to both input and output data, and varies the ending latent variable to obtain the optimal number of latent variables which result in the minimum RMSE. Typically, pretreatments on the data are done in an attempt to maximize differences due to sample differences and minimize differences from other sources such as normalization, mean-centering, and/or other appropriate standardization techniques. This is done to create an equal variance between all input data. While all of the wavelengths possess the same units, it is still important to process the data this way for cross comparison of other measurements and future studies.

PLS has been used not only on a variety of LIBS spectra in science, but rather commonly on problems in the nuclear industry such as the detection of thorium in spent fuel[58,59]. These empirical modeling techniques are tools for recognizing patterns and relationships between the input and output matrices, X and Y. They do not consider variables such as quality of sample, temperature effects, plasma physics, or any other attention to sampling parameters[60]. Thus, it is important to have a thorough discussion of the raw data and all spectra prior to conducting these analyses to account for discrepancies that may arise from the experimental set up, or possibly from material synthesis. The need to reduce the large arrays presented through unfiltered spectra have been noted in the literature and the initial approaches to this issue all center around omitting wavelengths

where intensities are weak or nonexistent[59,60]. This will be explored if necessary but excluding data can sometimes corrupt the predictive capabilities of PLS models. For example, the spectral range can be narrowed to include only areas pertaining to the known composition of the NUGETS, but if an unknown sample was shot with constituents outside of the elected range, classification of such sample would not be accurate. Additionally, all known spectral interferences can be removed from the model input data since there is not a definitive way to reduce these interferences during but doing so could lead to removal of rare emission lines.

Considerable effort will be directed towards establishing a catalog of submodels similar to that outlined in [37] Anderson *et al.* This will consist of obtaining at minimum, 20 geological standards with compositions bracketing those of the NV1X series of NUGETS. A minimum of 20 shots in 3-5 locations for each standard will be collected with the HHLIBS at a constant set of measurement parameters (gate delay, etc.). These measurements will be utilized to create submodels using PLS, which will be inputted into a larger PLS program that will be able to linearly interpolate the composition of the unknown NUGETS. This is a method that has been successfully implemented for ChemCam measurements on Mars geological samples and is anticipated to be successful in this approach.

Chapter 6

MVA techniques applied to NUGETS spectra (HHLIBS)

6.1 Abstract

6.2 Introduction

6.3 Experimental Setup

6.4 Results

6.4.1 Inductively Coupled Plasma Mass Spectrometry

6.4.2 Laser Induced Breakdown Spectroscopy

6.4.3 Partial Least Squares Regression Model

6.5 Discussion

Did research answer Objective III: Modifying data acquisition of HHLIBS in element identification of nuclear debris (post-detonation) through MVA techniques? Research goal III involves studies that are structured to answer the following: How can the spectra obtained from uncalibrated HHLIBS measurements be quantified to obtain compositional information? To what extent does the form of sample influence the accuracy of MVA models (powder, glass, etc.)? The hand held LIBS contains a 3B laser with a wavelength of 1064 nm and an average power of 3.8E-01 W, capable of operating with no sample preparation, no calibration, and at ambient conditions. This is ideal for measuring nuclear debris rapidly on-site. However, running the measurements with no calibration produce a highly qualitative relative abundance value for each element. Matrix effects such as spectral interferences confuse the spectra further, leading to a lack of confidence in the analysis. In order to extract useful information out of these spectra and manage the issues associated with matrix effects, multivariate data analysis (MVDA/MDA) techniques such as principal component analysis (PCR) and partial least squares regression (PLSR) are employed on

raw spectral data. To accomplish this research goal, a commercially available HHLIBS (SciAps Z300 LIBS) will be utilized to measure the NV1X series of NUGETS. A complex PLS model will then be utilized which considers a variety of geological standards for interpolation of spectral data as it correlates to composition. This model will be verified through chemically digesting samples using ammonium biflouride (ABF) digestion and subsequent characterizing through ICP-OES to obtain ppm level accuracy of the NV1X series composition.

Chapter 7

Conclusion

The overarching goal of this Ph.D. research is to develop rapid and effective techniques for studying pre- and post-detonation material. While the current nuclear forensic community is familiar with many of the individual techniques outlined in this paper, the combination of which are new and unique (Raman spectroscopy and IRMS, irradiation *then* subsequent oxidation, HHLIBS and MVA, ammonium biflouride digestion with ICP-OES). Very few studies have explored the potential of these interdisciplinary techniques, especially towards the characterization of nuclear materials. This research proposal seeks to fulfill the set goals and answer the following queries.

Acknowledgement

This work was supported by the U.S. Department of Homeland Security (DHS) Domestic Nuclear Detection Office (DNDO) Academic Research Initiative (ARI) under Grant 2015-DN- 077-ARI093. The views presented in this paper are those of the authors do not necessarily reflect those of U.S. Dept. of Homeland Security (DHS), DNDO, or the ARI. This material is also based upon work supported under an Integrated University Program Graduate Fellowship. Any opinions, findings, conclusions or recommendations expressed in this publication are those of the author(s) and do not necessarily reflect the views of the Department of Energy Office of Nuclear Energy.

Bibliography

1. Campbell, Keri, *et al.* "Synthesis and Characterization of surrogate nuclear explosion debris: urban glass matrix" *Journal of Radioanalytical and Nuclear Chemistry*, 314 (1), 197-206, (2017).

2. Mayer, K. *et al.* "Nuclear forensic science: correlating measurable material parameters to the history of nuclear material," *Chem. Rev.,* 113, 884–900, (2013).

3. Massachusetts Institute of Technology, "Spectroscopy History: The Era of Classical 32. Spectroscopy," http://web.mit.edu/spectroscopy/history/history-classical.html

4. Bursey, Maurice M. "A brief history of spectroscopy" *Access Science: Chemistry,* (2017).

5. Thomas, Nicholas C. "The Early History of Spectroscopy" *Journal of Chemistry Education,* 68(8), 631-634, (1991).

6. Hecker, Siegfried S., Martz, Joseph C., "Aging of Plutonium and Its Alloys" Los Alamos Science number 26, pages 238-243, (2000). http://permalink.lanl.gov/object/tr?what=info:lanl-repo/lareport/LA-UR-00-2619

7. Brown, John B., *et al.* "Fractionation of Oxygen Isotopes in the Formation of Oxide Films on Copper" *The Journal of Chemical Physics* 27, 251, (1957).

8. Jürgen H. Gross, "Mass Spectrometry - A Textbook" 3rd Edition: http://ms-textbook.com/

9. Skoog, Holler, Nieman, "Principles of Instrumental Analysis," *Saunders,* Chapter 18.

10. Nathalie Baclet, Marion Dormeval, Pascal Pochet, Jean-Marc Fournier, Franck Wastin, Eric Colineau, Jean Rebizant & Gerard Lander (2002) Self-irradiation effects in plutonium alloys stabilized in the δ-phase, Journal of Nuclear Science and Technology, 39:sup3, 148-151, DOI: 10.1080/00223131.2002.10875430

11. Chung, Brandon & Lema, K.E. & Allen, P.G.. (2015). Effects of self-irradiation in plutonium alloys. Journal of Nuclear Materials. 471. . 10.1016/j.jnucmat.2015.09.028.

12. "Plutonium Crystal Phase Transitions." *Plutonium Crystal Phase Transitions*. GlobalSecurity.org, 24 July 2011. Web. 07 June 2016. \ <http://www.globalsecurity.org/wmd/intro/pu-phase.htm>.

13. Haschke, John M., *et al.* "Surface and Corrosion Chemistry of Plutonium" *Los Alamos Science,* 26, 252-273, (2000).

14. Stakebake, J.L. "The High Temperature Oxidation of Plutonium-3.3 a/o Gallium" *Journal of Electrochem. Soc.: Solid State Science and Technology*, 124 (3), 460-465, (1977).

15. Jörg Boxhammer, Shorter test times for thermal- and radiation-induced ageing of polymer materials: 1: Acceleration by increased irradiance and temperature in artificial weathering tests, Polymer Testing, Volume 20, Issue 7, 719-724 (2001)

16. Wright, Richard N., "Summary of Studies of Aging and Environmental Effects on Inconel 617 and Haynes 230" Idaho National Laboratory, (2006).

17. Wang, Jing, *et al.*, "Combined effects of surface oxidation and interfacial intermetallic compound growth on solderability degradation of electrodeposited tin thin films on copper substrate due to isothermal ageing" *Corrosion Science*, 139, 383-394, (2018).

18. Gavgali, M., *et al.*, "The effects of artificial aging on wear properties of AA 6063 alloy" *Material Letters,* 57, 3713-3721, (2003).

19. Bigeleisen, J. "Chemistry of Isotopes", *Science* 147, 463-471, (1965).

20. Landolt-Börnstein, "Cupric Oxide (CuO) crystal structure, lattice parameters," *Non-Tetrahedrally Bonded Elements and Binary Compounds,* 41(C), (1998).

21. Kroopnick, P., & Craig, H., "Atmospheric oxygen: isotopic composition and solubility fractionation" *Science*, *175*(4017), 54-55, (1972).

22. Wolfer, Wilhelm G., “Radiation Effects in Plutonium: What is known? Where should we go from here?” *Los Alamos Science*, 26, (2000).

23. R. E. Stoller, M. B. Toloczko, G. S. Was, A. G. Certain, S. Dwaraknath, and F. A. Garner, On the use of SRIM for computing radiation damage exposure, Nucl. Instruments Methods Phys. Res. Sect. B Beam Interact. with Mater. Atoms, vol. 310, pp. 7580, 2013.

24. Naundorf, V, *et al.*, “Production rate of freely migrating defects for ion irradiation,” *Journal of Nuclear Materials,* 186, 227-236, (1992).

25. Varga, Zsolt, *et al.* “Plutonium age dating (production date measurement) by inductively coupled plasma mass spectrometry” *Journal of Radioanalytical Nuclear Chemistry,* 309, 1919-1926, (2016).

26. Kristo, Michael J., *et al.* “Nuclear Forensic Science: Analysis of Nuclear Material Out of Regulatory Control” *Annual Review of Earth and Planetary Sciences,* 44, 555-79, (2016).

27. Stratz, S. Adam, *et al.* “Modern Advancements in Post-Detonation Nuclear Forensic Analysis” *International Journal of Nuclear Security*, 2 (3), (2016).

28. Giminaro, Andrew V. *et al.* “Compositional planning for development of synthetic urban nuclear melt glass,” *Journal of Radioanalytical Nuclear Chemistry,* 306, 175-181, (2015).

29. Molgaard, Joshua, *et al.* “Development of synthetic nuclear melt glass for forensic analysis,” *Journal of Radioanalytical Nuclear Chemistry,* 304, 1293-1301, (2015).

30. Nizinski, Cody A., *et al.* “Production and Characterization of Synthetic Urban Nuclear Melt Glass,” *Journal of Radioanalytical Nuclear Chemistry*, 314, 2349-2355, (2017).

31. Gilbreath, Robert Boone, “Development of Nuclear Underground Engineered Test Surrogates for Technical Nuclear Forensics Exploitation,” *University of Tennessee, Knoxville,* Master Theses, (2017).

32. Seybert, Adam G. *et al.* "Preliminary investigation for the development of surrogate debris from nuclear detonations in marine-urban environments," *Journal of Radioanalytical Nuclear Chemistry*, 314, 77-85, (2017).

33. National Institute of Standards and Technology, Standard Reference Material 610 website: https://www-s.nist.gov/srmors/viewTableH.cfm?tableid=90

34. Hubley, *et al.* "FY18 Year-End Report: Green Chemistry – Dissolution of Post-Detonation Debris with Solid ABF LA-UR-18-30249"

35. Hubley NT, Brockman JD, Robertson JD (2017) Evaluation of ammonium bifluoride fusion for rapid dissolution in post-detonation nuclear forensics analysis. Radiochim Acta. 105:629-635

36. Clegg, Samuel M, *et al.* "Recalibration of the Mars Science Laboratory ChemCam instrument with an expanded geochemical database" *Spectrochimica Acta Part B*, 129, 64-85, (2017).

37. Anderson, Ryan B, *et al.* "Improved accuracy in quantitative laser-induced breakdown spectroscopy using sub-models" *Spectrochimica Acta Part B,* 129, 49-57, (2017).

38. Lappin, Derry, *et al.* "An experimental study of electrochemical polishing for micro-electrodischarge-machined stainless-steel stents" *Jrnl. Of Mat. Sci.: Mat. In Med.*, 23(2), 349-356, (2012).

39. L.M. Garrison, G.L. Kulcinski, The effects of tungsten's pre-irradiation surface condition on helium-irradiated morphology, J. Nucl. Mater. 466 (2015) 302-311.

40. ASTM E521

41. Meier-Augenstein, W. "Applied gas chromatography coupled to isotope ratio mass spectrometry" *Journal of Chromatography A*, 842, 351-371, (1999).

42. Benson, Sarah, *et al.* "Forensic applications of isotope ratio mass spectrometry – A review," *Forensic Science International,* 157, 1-22, (2006).

43. Howa, John D., *et al.* "Isolation of components of plastic explosives for isotope ratio mass spectrometry" *Forensic Chemistry,* 1, 6-12, (2016).

44. Benson, Sarah, *et al.* "Forensic analysis of explosives using isotope ratio mass spectrometry (IRMS) – Discrimination of ammonium nitrate sources" *Science and Justice*, 49, 73-80, (2009).

45. Varga, Zsolt, *et al.* "Methodology for the Preparation and Validation of Plutonium Age Dating Materials" *Analytical Chemistry,* 90, 4019-4024, (2018).

46. Gentile, N., *et al.* "On the use of IRMS in forensic science: Proposals for a methodological approach" *Forensic Science International*, 212(1-3), 260-271, (2011).

47. Princeton Instruments "Raman Spectroscopy Basics" *1-5.* *http://web.pdx.edu/~larosaa/Applied_Optics_464-564/Projects_Optics/Raman_Spectrocopy/Raman_Spectroscopy_Basics_PRINCETON-INSTRUMENTS.pdf*

48. Villa-Aleman, Eliel, *et al.* "Characterization of uranium tetrafluoride (UF4) with Raman spectroscopy," *Journal of Raman Spectroscopy,* 47 (7), 865-870, (2016).

49. Rondahl, Stina Holmgren, *et al.* "Comparing results of X-ray diffraction, A mu-Raman spectroscopy and neutron diffraction when identifying chemical phases in seized nuclear material, during a comparative nuclear forensics exercise" *Journal of Radioanalytical and Nuclear Chemistry*, 315 (2), 395-408, (2018).

50. Shiryaev, Andrey A. *et al.* "Forensic study of early stages of the Chernobyl accident: Story of three hot particles" *Journal of Nuclear Materials,* 511, 83-90, (2018).

51. Rickert, K. *et al.* "Assessing UO_2 sample quality with μ-Raman spectroscopy" *Journal of Nuclear Materials,* 514, 1-11, (2019).

52. Elorrieta, J.M., *et al.* "Temperature dependence of the Raman spectrum of UO_2" *Journal of Nuclear Materials,* 503, 191-194, (2018).

53. Radboud University, "General Instrumentation: ICP-OES" website: https://www.ru.nl/science/gi/facilities-activities/elemental-analysis/icp-oes/

54. Russo, Richard E., et al. "Laser Ablation in Analytical Chemistry" Analytical Chemistry, 85, 6162-6177, (2013).

55. Manard, Benjamin T., et al. "Laser ablation - inductively couple plasma - mass spectrometry/laser induced breakdwon spectroscopy: a tandem technique for uranium particle characterization" Journal of Analytical Atomic Spectrometry, (2017).

56. Krachler, Michael, et al. "Spatial distribution of uranium isotopes in solid nuclear materials using laser ablation multi-collector ICP-MS" Microchemical Journal, 140, 24-30, (2018).

57. Jamie Coble, "Partial Least Squares Regression" Fall 2019 Course NE 576: Empirical Modeling and Diagnostics, University of Tennessee, Knoxville.

58. Clegg, Samuel M., et al. "Multivariate analysis of remote laser-induced breakdown spectroscopy spectra using partial least squares, principal component analysis, and related techniques" Spectrochimica Acta Part B, 64, 79-88, (2009).

59. Unnikrishnan, V.K, et al. "Calibration based laser-induced breakdown spectroscopy (LIBS) for quantitative analysis of doped rare earth elements in phosphors" Materials Letters, 107, 322-324, (2013).

60. Singh, Manjeet, et al. "Analytical spectral dependent partial least squares regression: a study of nuclear waste glass from thorium based fuel using LIBS" Journal of Analytical Atomic Spectrometry, 30, 2507, (2017).

61. Hagemann, H. *et al.* Raman Spectra of Single Crystal CuO, Solid State Communications, Vol. 73. No. 6, pp. 447-451, 1990.

62. Levitskii V S, Shapovalov V I, Komlev A E *et al.* Raman Spectroscopy of Copper Oxide Film Deposited by Reactive Magnetron Sputtering, ISSN1063-7850, Technical Physics Letters, 2015, Vol. 41, No. 11, pp. 1094–1096. ©Pleiades Publishing, Ltd., 2015.

63. Zheng, Yao-Ting *et al.* In-situ Raman monitoring of stress evaluation and reaction in Cu2O oxide layer, Materials Letters, Volume 78, 2012, Pages 11-13, ISSN 0167-577X, https://doi.org/10.1016/j.matlet.2012.03.015.